Journal of Power Sources 604 (2024) 234416

Contents lists available at ScienceDirect

Journal of Power Sources

journal homepage: www.elsevier.com/locate/jpowsour

$NdMn_{1.5}Ru_{0.5}O_5$, a high-performance electrocatalyst with low Ru content for acidic oxygen evolution reaction

Isabel Rodríguez-García [a], José Luis Gómez de la Fuente [a], Jorge Torrero [b], Daniel García Sánchez [b], Mohamed Abdel Salam [c], José Antonio Alonso [d], Aldo Saul Gago [b], Kaspar Andreas Friedrich [b], Sergio Rojas [a,*], María Retuerto [a,**], Álvaro Tolosana-Moranchel [a,***]

[a] Grupo de Energía y Química Sostenibles, Instituto de Catálisis y Petroleoquímica, CSIC, C/Marie Curie 2, 28049, Madrid, Spain
[b] Institute of Engineering Thermodynamics/Electrochemical Energy Technology, German Aerospace Center (DLR), Pfaffenwaldring 38-40, 70569, Stuttgart, Germany
[c] Chemistry Department, Faculty of Science, King Abdulaziz University, P. O Box 80200, Jeddah, 21589, Saudi Arabia
[d] Instituto de Ciencia de Materiales de Madrid, CSIC, C/Sor Juana Inés de la Cruz 3, 28049, Madrid, Spain

HIGHLIGHTS

- $NdMn_{1.5}Ru_{0.5}O_5$ exhibits OER activity in acidic media of 500 A g_{Ru}^{-1}@1.5 V.
- Stable PEMWE with $NdMn_{1.5}Ru_{0.5}O_5$ anode (0.5 $mg_{Ru}cm^{-2}$) achieved 1.97 V@0.5 A cm^{-2}
- $NdMn_{1.5}Ru_{0.5}O_5$ shows bifunctional OER/ORR activity, with a BI of 0.88 V.

GRAPHICAL ABSTRACT

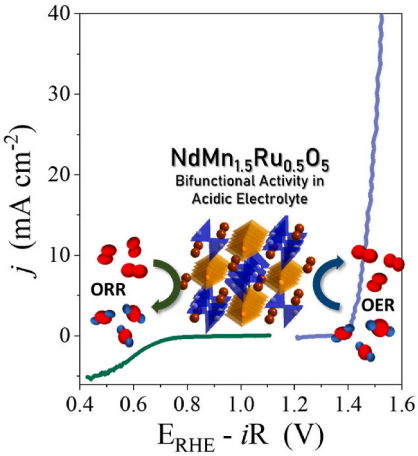

ARTICLE INFO

Keywords:
Clean hydrogen
Water electrolysis
PEMWE
Ru mixed oxide
Ir-free anode
Bifunctional catalyst

ABSTRACT

A mixed oxide with the crystal structure of the $DyMn_2O_5$ family, namely $NdMn_{1.5}Ru_{0.5}O_5$, is reported active for the oxygen evolution reaction (OER) in acidic media. $NdMn_{1.5}Ru_{0.5}O_5$ displays high OER activity of 500 A g_{Ru}^{-1} at 1.5 V. Moreover, is more stable than most Ru oxides reported to date, remaining active for more than 500 cycles between 1.1. and 1.7 V at low scan rate of 10 mV s^{-1}. The high activity and stability are attributed to the Ru cations, as $NdMn_2O_5$ exhibits very low OER activity. $NdMn_{1.5}Ru_{0.5}O_5$ has particularly short Ru–Ru distances of 2.60 Å, a value close to the Ru–Ru metallic distances around 2.642 Å. The high activity and durability of

* Corresponding author.
** Corresponding author.
*** Corresponding author.
E-mail addresses: srojas@icp.csic.es (S. Rojas), m.retuerto@csic.es (M. Retuerto), alvaro.tolosana@csic.es (Á. Tolosana-Moranchel).

https://doi.org/10.1016/j.jpowsour.2024.234416
Received 4 December 2023; Received in revised form 22 March 2024; Accepted 22 March 2024
Available online 6 April 2024

$NdMn_{1.5}Ru_{0.5}O_5$ for the OER are also demonstrated in a proton exchange membrane water electrolysis cell by producing a low-loaded anode electrode with 0.5 $mg_{Ru}cm^{-2}$. The cell achieves 1.97 V at 0.5 A cm^{-2}, consistent with the performances reported for Ru-based catalysts but with lower Ru loading. This performance is maintained during 100 h of operation. Additionally, $NdMn_{1.5}Ru_{0.5}O_5$ displays visible ORR activity in acidic media, recording an onset potential of 0.85 V at 0.1 mA cm^{-2}. It is noteworthy to highlight the extreme rarity of bifunctional ORR/OER catalysts acidic media.

1. Introduction

Water electrolysis is considered as the technology of choice for producing H_2 from decarbonized renewable electricity [1,2]. The overall electrochemical reaction for water splitting comprises two half-cell reactions: the oxygen evolution reaction (OER) and the hydrogen evolution reaction (HER). The kinetics for the OER are notably slow, proceeding at measurable rates (current) when the potential is driven away from equilibrium (overpotential) towards more positive potentials, E > 1.23 V. Among electrolysis technologies, proton exchange membrane water electrolysis (PEMWE) offers several advantages for H_2 production from renewable electricity. It has a very fast response, enabling adaptation to fluctuations in solar and wind energy. PEMWE achieves high current densities at moderate voltages, yielding highly pure H_2 that can be pressurized within the system [1,2].

However, the harsh conditions of the OER, such as high potential, low local pH, and high oxygen species content, ultimately determine the materials suitable for use in PEMWEs. To date, IrO_x-based catalysts are the only ones capable of withstanding those harsh conditions in the anode electrode [3,4]. Nevertheless, there is an ongoing debate about whether the scarcity and high cost of Ir (around 4600 $/troy oz) may restrict the large-scale production, in the terawatt (TW) scale, of PEMWEs [5,6]. Recently, it has been proposed that increasing Ir-specific power density to around 0.1 mg_{Ir}/W, from today's values ranging between approximately 0.34 to 2.0 mg_{Ir}/W, along with Ir recycling, could enable the implementation of PEMWE technology at the TW scale by 2050 [7]. This would only be possible by combining the development of advanced electrocatalysts, such as mixed oxides of Ir and/or Ru [4,8,9], while optimizing the structure of other electrolyzer components, including porous transport layers (PTLs) and membranes [10].

A promising approach is to replace Ir with Ru, as it could potentially reduce the cost of the anode electrode by up to one order of magnitude, given that the price of Ru is approximately 465 $ per troy oz [5]. Additionally, this substitution would broaden the range of elements utilized in the anode of PEMWEs. Recently, Ru oxides and mixed oxides have demonstrated activity for the OER in acidic media [11]. However, in many instances, their durability is notably low due to the potential-induced transformation of stable Ru^{4+} to unstable $Ru^{>4+}$ [12–14], resulting in its dissolution in the electrolyte. Several strategies are currently being explored to enhance the activity and, especially, the durability of Ru electrocatalysts for the OER. For example, Ru oxide has been modified to maximize its exposed surface area in structures such as nanoparticles or nanosheets [15,16], ultimately leading to the design of catalysts based on Ru single atoms [17]. RuO_2 doping with cations of certain elements such as Sn, W, Ti, etc., has shown success in improving catalytic performance and durability [18–22]. Particularly, the introduction of Nd into RuO_x has been reported to stabilize high-valence Ru cations, preventing the dissolution of Ru during the OER [23]. In some cases, Ru has been used as a promoter rather than the active phase, such as in Ru–MnO_2 [24].

Mixed oxides are garnering considerable attention as electrocatalysts for the OER [4]. Concerning Ru-mixed oxides, perovskites like $SrRuO_3$ exhibit very high activity but low durability [12,13,25]. Efforts to improve their stability have been addressed by partial doping with monovalent cations such as Na^+ or K^+ [26,27], resulting in increased OER activity and durability, as well as the design of complex structures like the quadruple perovskite $CaCu_3Ru_4O_{12}$ [28]. Currently, Ru pyrochlores are probably the most promising Ru-mixed oxides for the OER, boasting significantly higher durability than perovskites while also exhibiting high activity [29–36]. Furthermore, it's worth noting that some platinum group metal (PGM)-free electrocatalysts for the OER in acidic electrolyte, particularly Mn-oxides typically doped with elements like Fe, Co, Sn, etc., have been shown OER activity [37]. However, these Ru-free Mn-based catalysts are usually evaluated under operation conditions far from those suitable for PEMWEs, namely low current densities, ≤10 mA cm^{-2}, with only a few studies conducted at a current density of 100 mA cm^{-2} or higher [38–40].

It is not uncommon for metal oxide-based electrocatalysts to display bifunctional activity in alkaline electrolyte. This means that they possess both OER activity and activity for the oxygen reduction reaction (ORR) in alkaline conditions. However, it is extremely rare for metal oxides to show ORR activity, and even less common for them to exhibit combined ORR and OER activity, in acidic electrolyte. To the best of our knowledge, only certain Ti- and Zr-based oxides have been reported to be active for the ORR in acidic electrolyte [41–44]. Furthermore, only F–$Cu_{1.5}Mn_{1.5}O_4$ and $Cu_2MnO_4{\cdot}H_2O{\cdot}OFx$ have been reported to be active for both the OER and the ORR in acidic electrolyte, with bifunctional indexes (BI) of 0.75 and 1.4 V, respectively [45,46].

In this study, we present the mixed oxide $NdMn_{1.5}Ru_{0.5}O_5$ as an electrocatalyst for the OER in acidic electrolyte, which also exhibits activity for the ORR. The material is isostructural with $DyMn_2O_5$ (space group *Pbam*) and contains infinite chains of $(Mn,Ru)^{4+}O_6$ octahedra sharing edges, linked by dimeric $(Mn)^{3+}O_5$ units. The crystal structure shows a contraction of the *c* axis, with Ru–Ru distances between the octahedra resembling those found in metallic Ru. The high OER activity and durability of $NdMn_{1.5}Ru_{0.5}O_5$ is attributed to the occupation of Ru atoms in octahedral sites, and probably promoted by the Ru–Ru metallic-like distances. Additionally, our study demonstrates that $NdMn_{1.5}Ru_{0.5}O_5$ also displays activity for the ORR in acidic electrolyte, resulting in a bifunctional catalyst with a BI of 0.88 V, which is among the lowest reported in the literature.

2. Experimental

2.1. Synthesis of $NdMn_{1.5}Ru_{0.5}O_5$ mixed oxide

$NdMn_{1.5}Ru_{0.5}O_5$ was synthesized using the citrate technique, following a protocol outlined elsewhere [47]. Initially, stoichiometric amounts of the oxide precursors −0.5028 g of Nd_2O_3 (Aldrich, 99.9%), 0.5124 g of $MnCO_3$ (Aldrich, ≥ 99.9%) and 0.1977g of RuO_2 (Aldrich 99.9%)-were dissolved in 100 mL of a citric acidic solution (0.52 M) with 5 mL of HNO_3 (Alfa Aesar, 68–70%), under vigorous magnetic stirring. Subsequently, the suspension was evaporated at approximately 100 °C, resulting in an organic resin with homogeneously distributed cations. The mixture was then dried at 140 °C and subjected to a thermal treatment in a horizontal furnace under static air at 600 °C (heating ramp of 2 °C min^{-1}) for 12 h and 800 °C (heating ramp of 1.67 °C min^{-1}) for 2 h. Finally, the solid was annealed at 800 °C for an additional 12 h in air.

2.2. Catalyst physicochemical characterization

The crystal structure of $NdMn_{1.5}Ru_{0.5}O_5$ was analyzed using an X-ray polycrystal PANalytical X'Pert PRO with CuKα radiation (1.541874 Å).

Diffractograms were obtained with a step size of 0.04° and an accumulation time of 20 s per point. The refinement of the crystal structures was performed using the Rietveld method and the Fullprof crystallographic program [48,49].

XPS measurements were conducted using a customized SPECS apparatus equipped with a non-monochromatic X-ray source XR 50 and a hemispherical energy analyzer PHOIBOS 150. X-ray Mg K-line (1253.6 eV) was used as excitation source (operating at 200 W/12 kV). Survey spectra, as well as the energy regions of the elements under study (Ru 3*d*, Mn 2*p*, and Nd 3*d*) were scanned at increments of 0.1 eV and a fixed pass energy of 20 eV. Charge effects were accounted for by setting the C 1*s* core-level peak at 284.6 eV. The obtained spectra were analyzed using XPS Casa Software and a combination of Lorentzian and Gaussian peak shapes. A Shirley-type background was used for peak analysis.

TEM micrographs were obtained using a JEOL 2100HT microscope at 200 kV. The microscope is equipped with an INCA OXFORD detector for compositional analysis through X-Ray Energy Dispersive Spectroscopy, EDS. The deposition was carried out by preparing a highly diluted suspension of the catalyst under investigation in ethanol.

An Inductively Coupled Plasma (ICP) Atomic Emission Spectrometer PERKIN ELMER mod. OPTIMA 2100 DV was used for the analyses. Samples for analysis consisted of electrolyte collected *post-mortem*, along with a blank containing 0.1 M $HClO_4$ electrolyte.

2.3. Electrochemical characterization

The OER and ORR performances of the $NdMn_{1.5}Ru_{0.5}O_5$ catalyst were initially assessed in acidic electrolyte using a rotating disk electrode (RDE). Experiments were conducted using a three-electrode cell with an Ag/AgCl (3 M) reference electrode and a graphite rod as the counter electrode. The reference electrode was calibrated by recording the hydrogen evolution reaction in an H_2-saturated 0.1 M $HClO_4$ electrolyte, using a Pt wire as the working electrode. The electrolyte employed in this study, namely 0.1 M $HClO_4$, was prepared with $HClO_4$ (Sigma Aldrich; 70%) and MilliQ water (18.2 MΩcm). Electrochemical measurements were conducted with an Autolab PGSTAT320 N potentiostat/galvanostat controlled by the NOVA 2.1 software. Unless otherwise specified, potentials are reported versus the reversible hydrogen electrode (RHE), and are *i*R-corrected by using the high-frequency resistance value of 24 Ω measured by electrical impedance spectroscopy (EIS) at open circuit voltage in 0.1 M $HClO_4$.

For the electrochemical measurements, the desired quantity of $NdMn_{1.5}Ru_{0.5}O_5$ was deposited on a 0.196 cm^2 glassy carbon RDE (Pine Instruments) as an ink. Prior to deposition, the electrode was polished with alumina slurry (0.05 μm, PINE) to achieve a mirror ending and then rinsed with triple-distilled water. The ink containing the catalyst was prepared by dispersing 5 mg of $NdMn_{1.5}Ru_{0.5}O_5$ and 1 mg of carbon black Vulcan-XC-72R (note that carbon Vulcan is used to ensure a better dispersion of the ink) into 970 μL tetrahydrofuran (THF) and 30 μL of Nafion 117 solution (5%) with an Ultrasonic mixer UP50H (Hielscher). The catalyst loading on the electrode was 0.38 mg cm^{-2}.

The OER and ORR polarization curves were obtained by recording consecutive cyclic voltammograms (CVs) between 1.2 and 1.7 V (OER) and 1.1 and 0.4 V (ORR) in O_2-saturated electrolyte at a scan rate of 10 mVs^{-1} and 1600 rpm. Following the ORR measurement, a blank voltammogram is recorded in Ar-saturated electrolyte without rotation and used to correct the double layer contribution. Pure Faradaic currents were calculated by subtracting the anodic sweeps of the ORRcurrent and the capacitive current (see Supporting Information). For the assessment of the production of O_2 during the OER and the production of H_2O_2 during the ORR, a rotating ring disk electrode (RRDE) with a Pt ring, was used. Further details are given in the supplementary information section.

For the post-mortem studies, $NdMn_{1.5}Ru_{0.5}O_5$ was deposited onto a Toray™ Carbon Paper (Quintech, TP-060-T20) without Nafion to avoid contamination of the XPS chamber. The catalyst loading was 2.5 $mg_{catalyst}$ cm^{-2} and the area of the electrode was 0.5 cm^{-2}. CVs were recorded in O_2-saturated electrolyte at 10 mVs^{-1} (the electrolyte was stirred continually) in the potential range of each reaction. Specimens for post-mortem TEM analysis were collected by gently scratching the carbon paper after the desired number of cycles.

$NdMn_{1.5}Ru_{0.5}O_5$ was tested as the anode in a PEMWE cell with an active area of 4 cm^2. To assemble the catalyst-coated membrane (CCMs), a wet spraying approach was employed. The catalyst was deposited onto a Nafion 212 membrane placed onto a vacuum heating table (Fuel Cell Store) heated at 100 °C during catalyst deposition. Throughout the deposition process, the distance between the spraying nozzle and the membrane was maintained at approximately 6 cm, resulting in an ink deposition rate of 2–3 min mL^{-1}. The ink used for catalyst deposition contained 10 mg of $NdMn_{1.5}Ru_{0.5}O_5$ in 1 mL of ultra-pure H_2O (MiliQ, 18 MΩ cm^{-1}) and Nafion® D521 solution (5 wt% in lower aliphatic alcohols and water), resulting in a final ionomer content of 25 and 30 wt % for the anode and cathode layers, respectively. This mixture was sonicated until the catalyst is properly dispersed. Additionally, 1 mL of isopropanol (IPA, ACS reagent, ≥99.5%) was added to the mixture and sonicated for 10 min until a well-dispersed and homogeneous ink was obtained. After spraying and drying, the CCM was hot pressed at 5 Mpa and 125 °C. A CCM with $NdMn_{1.5}Ru_{0.5}O_5$ (0.5 mg_{Ru} cm^{-2}) at the anode and Pt/C 40% (0.4 mg_{Pt} cm^{-2}) at the cathode was obtained and tested in a PEMWE setup optimized for screening cell components. PTLs used in both anode and cathode electrodes are Ti porous sintered layer (PSL). This is a Ti mesh on which a Pt coating produced by diffusion bonding is applied, resulting in PSL/Ti-PTL [50]. For better contact, untreated carbon paper (Spectracarb 2050A-1050) was placed between the cathode electrode and the PTL. Carbon paper is a state-of-the-art PTL material in PEM. Ti bipolar plates (Ti-BPPs) were employed on both the anode and cathode sides. The polarization curves were carried out galvanostatically at 80 °C and ambient pressure following the JRC EU-harmonized procedure [51], employing a dwell and consecutive recording period of 10 s for each current step. Polarization curves up to 0.5 A cm^{-2} and durability tests at a constant current density of 0.5 A cm^{-2} were recorded.

3. Results and discussions

3.1. Crystal structure of $NdMn_{1.5}Ru_{0.5}O_5$

$NdMn_{1.5}Ru_{0.5}O_5$ was obtained as a mixed oxide with the structure of $DyMn_2O_5$ (orthorhombic space group *Pbam*) [52]. The XRD patterns and the Rietveld refinement of the crystal structure of $NdMn_{1.5}Ru_{0.5}O_5$, along with a scheme of the crystal structure, are shown in Fig. 1. $NdMn_{1.5}Ru_{0.5}O_5$ is formed by infinite chains of $(Mn,Ru)^{4+}O_6$ edge-sharing octahedra, which are interconnected by dimeric $(Mn)^{3+}O_5$ squared pyramids and NdO_8 units. In addition, the refinement of the crystal structure reveals the presence of 5 % atomic Ru^{3+} in squared pyramids. As determined from the refinement of the crystal structure by XRD (Fig. 1), $NdMn_{1.5}Ru_{0.5}O_5$ presents short Ru/Mn–Ru/Mn distances of 2.60 Å between the octahedra, suggesting the presence of Ru–Ru metal bonding, since Ru–Ru distance in metallic Ru is 2.642 Å and Mn–Mn distance in metallic Mn is 2.34 Å [53,54]. Note that the distance of 2.60 Å is in good agreement with the distances previously reported for $NdMn_{1.5}Ru_{0.5}O_5$ from Neutron Powder Diffraction data [47].

3.2. OER and ORR activity of $NdMn_{1.5}Ru_{0.5}O_5$

Fig. 2a shows the positive-going scan of the cyclic voltammograms recorded in O_2-saturated 0.1 M $HClO_4$ with $NdMn_{1.5}Ru_{0.5}O_5$. The potential at which a current density of 10 mA cm^{-2} is obtained is usually taken as the metric to benchmark the OER activity of electrocatalysts [55]. $NdMn_{1.5}Ru_{0.5}O_5$ records 1.5 V at such current, hence ranking among the most active Ru or Ir electrocatalysts reported in the literature. To the best of our knowledge, this activity is only surpassed by

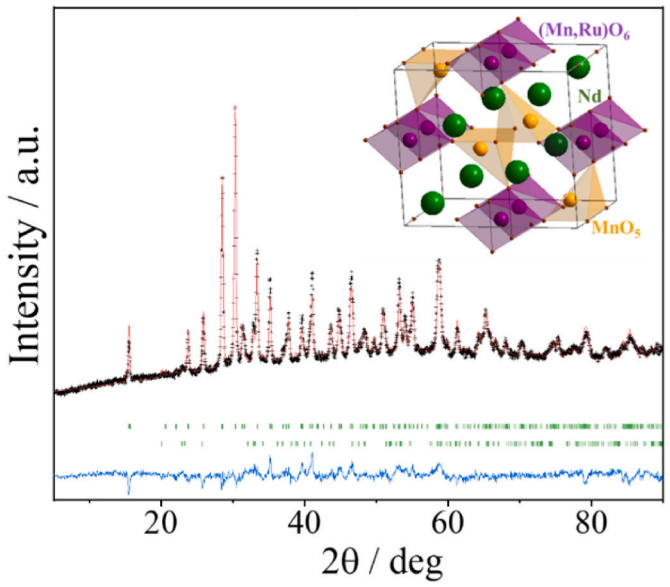

Fig. 1. XRD pattern (black crosses) and Rietveld refinements (red line) of the crystal structure of $NdMn_{1.5}Ru_{0.5}O_5$. The small reflection at 33° is 5(2) % of $NdMnO_3$ impurity. The blue line is the difference between the experimental and refinement, and the small green lines indicate the Bragg reflections of both crystallographic structures refined. Inset: Schematic view of the crystal structure of $NdMn_{1.5}Ru_{0.5}O_5$. (For interpretation of the references to colour in this figure legend, the reader is referred to the Web version of this article.)

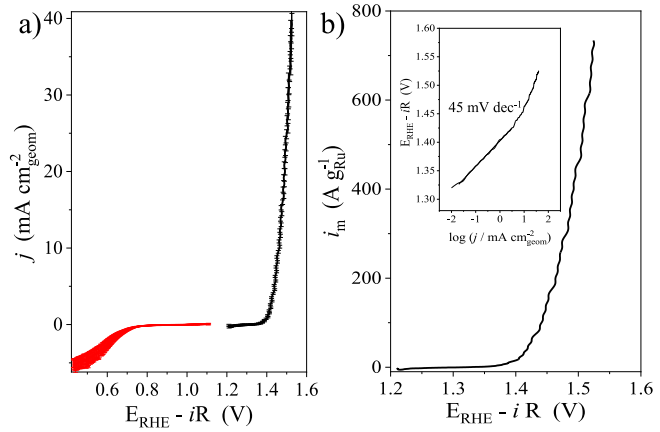

Fig. 2. a) OER (black curve) and ORR activity (red curve) of $NdMn_{1.5}Ru_{0.5}O_5$ at 10 mV s^{-1} and 1600 rpm in O_2-saturated 0.1 M $HClO_4$. b) OER Ru-mass-specific activity. Inset: Tafel plot from the OER polarization curves. (For interpretation of the references to colour in this figure legend, the reader is referred to the Web version of this article.)

$SrRuO_3$-based catalysts and $CaCu_3Ru_4O_{12}$ [26–28]. This is further illustrated in Table 1, which compiles the OER performance of the most active Ru and Ir mixed oxides for the OER in acidic electrolyte. A Tafel slope of 45 mV dec^{-1} is calculated for $NdMn_{1.5}Ru_{0.5}O_5$ between 1.35 and 1.45 V (inset of Fig. 2b). This value is very similar to the values typically reported for Ru catalysts, with Tafel slopes ranging between 40 and 60 mV dec^{-1}. Note that Ru Tafel slopes are lower than Ir ones (Table 1), indicating that the kinetics for the OER are faster on Ru-based electrocatalysts.

Fig. 2b shows the Ru-mass-normalized activity (i_M) of $NdMn_{1.5}Ru_{0.5}O_5$ for the OER, reaching a i_M of 500 A g_{Ru}^{-1} at 1.5 V. This i_M is among the highest in the literature, along with $Y_2[Ru_{1.6}Y_{0.4}]O_{7-\delta}$, $Y_{1.7}Sr_{0.3}Ru_2O_7$ and $CaCu_3Ru_4O_{12}$, that reach values of 700, 1018, and 1942 A g_{Ru}^{-1} at 1.55 V, respectively [28,35,56]. All of these Ru-based

Table 1
OER activity of the state-of-the-art Ir- and Ru- mixed oxide catalysts in acidic electrolyte.

Catalyst	Reference	E-*i*R (V) @ 10 mA cm^{-2}	Tafel slope (mV dec^{-1})	i_m (A $g_{Ru/Ir}^{-1}$) @1.55 V	Durability test
$NdMn_{1.5}Ru_{0.5}O_5$	This work	1.5	45	520	
$Y_{1.85}Zn_{0.15}Ru_2O_{7-\delta}$	[33]	1.521	36.9		After 2000 cycles bt. 1.35–1.6 V the activity decreases 36 %
$Y_2Ru_2O_{7-\delta}$	[32]	1.55	55	300	Stable 10000 cycles bt. 1.35 and 1.6 V @ 100 mV s^{-1}
$Nd_2Ru_2O_7$	[29]	1.58	41	~250	Loss of activity after ~ 6 h @ 1.56 V
$Y_2Ru_2O_7$	[29]	1.56	40	~300	Loss of activity after ~ 8 h @ 1.56 V
$Gd_2Ru_2O_7$	[29]	1.59	47	~200	Loss of activity after ~ 8 h @ 1.56 V
$Bi_2Ru_2O_7$	[29]	1.59	48	~200	Loss of activity after ~12 h @ 1.56 V
$Y_{1.7}Sr_{0.3}Ru_2O_7$	[35]	1.49	44.8	1018	
$Sr_{0.90}Na_{0.10}RuO_3$	[26]	1.4	40		Loss of 65% of initial activity after 80 cycles
$Sr_{0.95}K_{0.05}RuO_3$	[27]	1.37	69		56% of the initial activity is maintained after 20 cycles
$CaCu_3Ru_4O_{12}$	[28]	1.4	40	1942 @ 1.5 V	CP at 10 mA cm^{-2} for 24 h
Y_2MnRuO_7	[34]	1.5	47	700	45 h @ 10 mA cm^{-2}
Dy_2MnRuO_7	[34]	1.51	47		25 h @ 10 mA cm^{-2}
Tb_2MnRuO_7	[34]	1.54	56		15 h @ 10 mA cm^{-2}
RuO_2	[29]	1.63	77		CA at 1.56 V for 1h
Sr_2IrO_4	[65]	1.516	45	394	6 h @ 10 mA cm^{-2}

catalysts exhibit either the perovskite or the pyrochlore structure, which are currently the only Ru-mixed oxide structures reported active for the OER in acidic electrolyte. However, this is the first time that a Ru oxide with a crystal structure from the $DyMn_2O_5$ family is reported to display OER activity in acidic media. Therefore, to assess whether the oxidation current during the OER scans actually corresponds to the production of O_2, we used a rotating ring disk electrode (RRDE) setup to monitor the production of O_2. The results are shown in Fig. S1of the Supplementary Information (SI).

$NdMn_{1.5}Ru_{0.5}O_5$ is also active for the ORR in acidic media, a rare feature for oxide-based catalysts. This is a remarkable observation, since to date, most catalysts endowed with ORR activity in acid media are based on PtM/C (M = Co, Ni …) or single atom iron sites, coordinated to nitrogen atoms in a graphitic carbon network (Fe/N/C) [57–59]. To our knowledge, only certain Ti and Zr-based oxides have reported activity for the ORR in acidic electrolyte [41–44]. Fig. 2a shows the positive-going scan (background corrected) of the ORR polarization curve recorded in the O_2-saturated electrolyte (0.1 M $HClO_4$) at 10 mVs^{-1} and 1600 rpm for $NdMn_{1.5}Ru_{0.5}O_5$. As shown in Table S1, the E_{onset} and $E_{1/2}$ values of 0.85 and 0.56 V, respectively, compare well with the ORR activity reported for published oxides. Fig. S2a upper

panel shows the low production of H_2O_2, indicating that the ORR mainly proceeds through a 4 e^- pathway. Fig. S2b shows the ORR mass-normalized activity.

The bifunctional OER/ORR activity of $NdMn_{1.5}Ru_{0.5}O_5$ in acidic media is worth mentioning since several mixed oxides have been reported to display ORR/OER bifunctional activity in alkaline media [60–62]. However, to the best of our knowledge, only fluorinated Cu–Mn oxides are PGM-free bifunctional catalysts in acidic media [45,46]. The bifunctional index (BI) is defined as the difference between the potentials needed to reach 10 and -3 mA cm^{-2} ($BI = E_{OER,j\ 10} - E_{ORR,j-3}$) during the OER and ORR, respectively. $NdMn_{1.5}Ru_{0.5}O_5$ displays a BI of 0.88 V, showing a remarkable oxygen bifunctional performance comparable to that of Pt/C, Ru/C, and RuO_2/C, which are 1.02, 1.01 and 0.94 V, respectively [63,64]. F–$Cu_{1.5}Mn_{1.5}O_4$ and $Cu_2MnO_4{\cdot}H_2O{\cdot}OF_x$ display BIs of 0.75 and 1.4 V, respectively [45,46].

However, the durability of $NdMn_{1.5}Ru_{0.5}O_5$ during the ORR is relatively low, and the activity decays very fast after 60 cycles, see Table S1 and Fig. S3a. Therefore, further details concerning the activity and durability of $NdMn_{1.5}Ru_{0.5}O_5$ for the ORR, including activity and selectivity data in Fig. S2, durability, and the characterization of the used catalyst (Figs. S3 and S4) are described in the SI.

3.3. $NdMn_{1.5}Ru_{0.5}O_5$ durability for the OER

The durability of $NdMn_{1.5}Ru_{0.5}O_5$ during the OER has been evaluated by recording consecutive CVs between 1.1 and 1.7 V at 10 mV s^{-1}. As shown in Fig. 3a, the OER activity of the oxide remains stable during 500 cycles, with a loss of activity in terms of $\Delta E_{1\text{-}500}$, defined as the difference between the potential needed to reach 10 mA cm^{-2} at the 1st (E_1) and the 500th (E_{500}) cycle, of only 15 mV. A closer inspection of the polarization curves reveals a slight improvement of the initial activity during the first 200 cycles, $\Delta E_{1\text{-}200} = -10$ mV (note that the negative sign in the ΔE value indicates that the E_{200} is less positive than E_1). After 1000 cycles, the loss of the OER activity is more obvious, with a $\Delta E_{1\text{-}1000}$ of 60 mV at 10 mA cm^{-2}. However, 70% of the Ru mass-normalized activity is still maintained. Table 2 shows the evolution of the most relevant parameters of $NdMn_{1.5}Ru_{0.5}O_5$ for the OER during cycling.

In addition to the high OER activity, the long durability of $NdMn_{1.5}Ru_{0.5}O_5$ during the OER is a remarkable result since most Ru-based catalysts are only stable in the strong oxidant and acidic environment of the OER during a small number of cycles [13,26]. The most stable Ru mixed-oxides for the OER are those with the pyrochlore structure, which in some cases display OER activity for thousands of cycles [29,32,34]. For example, $Y_2Ru_2O_{7-\delta}$ remains stable for 10000 cycles between 1.35 and 1.6 V at 100 mV s^{-1} with no evident loss of activity [32]. However, Ru-based pyrochlores are less active than other Ru oxides, with potentials around 1.60 V to achieve 10 mA cm^{-2}. Note

Table 2
Activity parameters of $NdMn_{1.5}Ru_{0.5}O_5$ extracted from OER curves and mass activities results.

OER	E-*i*R (V) @ 10 mA cm^{-2}	*j* (mA cm^{-2}) @ 1.5 V	Tafel slope (mV dec^{-1})	i_M (A g_{Ru}^{-1}) @ 1.5 V
Cycle 1	1.46	23.22	45	460
Cycle 100	1.47	20.96	47	432
Cycle 200	1.45	26.93	47	497
Cycle 500	1.48	16.27	53	307
Cycle 1000	1.52	7.53	68	143

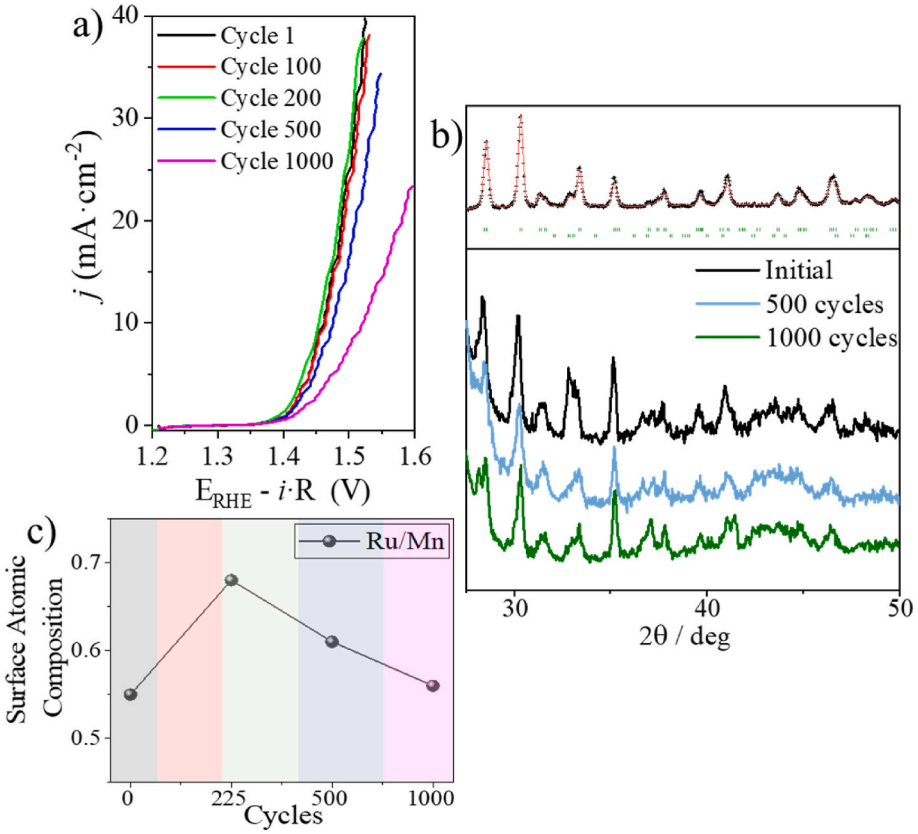

Fig. 3. a) Evolution of the OER polarization curves for $NdMn_{1.5}Ru_{0.5}O_5$ with cycles. (b) Comparison of the XRD patterns of the initial catalyst and of the catalyst recovered after 500 and 1000 OER cycles. Note that the XRD are for the catalysts deposited on carbon paper. c) Evolution of the Ru/Mn surface atomic composition during OER cycles as determined from XPS.

that $NdMn_{1.5}Ru_{0.5}O_5$ only needs 1.50 V to reach the same current density. On the contrary, Ru-based perovskites display higher OER activity than Ru pyrochlores but lack stability, usually losing their OER activity in less than 100 OER cycles [26,27]. To our knowledge, only the $CaCu_3Ru_4O_{12}$ perovskite is stable for the OER during 24 h at 10 mA cm^{-2} [28]. The differences in durability during the OER can be ascribed to structure/composition features. Thus, Ru perovskites usually have alkali metals such as Sr, Ca, and Ba in the A site. Such alkaline cations tend to dissolve quickly in acidic electrolyte, hence triggering catalyst deactivation during the first OER cycles [26,27]. On the other hand, Ru pyrochlores usually have rare earth elements in their structure, which have less basicity. As a consequence, their dissolution rate during the OER is lower and, therefore, they are more stable during the OER in acidic electrolyte [34]. Following this line of thinking, we can ascribe the high durability of $NdMn_{1.5}Ru_{0.5}O_5$ during the OER to the presence of Nd in its structure, which has been reported to prevent Ru dissolution during OER [23]. As for the origin of the high OER activity of $NdMn_{1.5}Ru_{0.5}O_5$, it can be ascribed to the combination of several features. Firstly, $NdMn_{1.5}Ru_{0.5}O_5$ contains Ru^{4+} cations in octahedral positions (see below), which have been reported to result in high OER activity [13,20,26,65]. Moreover, in a previous work, we demonstrated that the presence of Mn and Ru cations in mixed oxides results in a very active surface phase of Ru–*O*–Mn ensembles, endowed with high OER activity [34,66]. Another reason that accounts for the high OER activity is the short Ru–Ru distances of 2.60 Å between the octahedra, which is close to Ru–Ru distances of 2.642 Å found in metallic Ru, which is known to be highly active for the OER [67]. A similar behavior has been also reported for Ir oxides in which the oxides with Ir–Ir distances close to metallic Ir display high OER activity in acidic electrolyte [4,9,68–70].

3.4. Physicochemical characterization: initial catalyst and post-mortem after OER

To study the evolution of the catalyst's structure and composition during the OER, $NdMn_{1.5}Ru_{0.5}O_5$ is recovered after a number of consecutive OER cycles and thoroughly analyzed by XRD, XPS, and TEM. In addition, the amount of Ru, Mn, and Nd in the electrolyte after these cycles is analyzed by ICP. Fig. 3b compares the XRD patterns for the fresh catalyst and for the catalyst recovered after 500 and 1000 OER cycles (note that the diffractograms correspond to the catalysts deposited onto the carbon paper). As observed, the catalysts recovered after the OER cycles display diffractograms identical to those of the original compound. This suggests that the crystal structure of $NdMn_{1.5}Ru_{0.5}O_5$ remains unchanged throughout the reaction, even as the activity diminishes after 1000 cycles.

The oxidation state and relative atomic abundance of Ru, Mn and Nd cations at the surface of the fresh catalyst and of the electrocatalyst recovered after 225, 500 and 1000 OER cycles have been analyzed by XPS. In order to avoid the strong overlapping of the Ru 3*d* and C 1*s* core-level regions, we analyzed the Ru 3*p* core-level region. Note that since the XPS spectra were obtained from the catalyst deposited onto the carbon paper, the intensity of the C 1*s* region is very high. The spectra of the Ru $3p_{3/2}$, Mn $2p_{3/2}$, and Nd 3*d* core levels are shown in Fig. S4 in the SI. The Ru $3p_{3/2}$ peak (Fig. S4a) comprises three peaks centered at 460.0, 463.9, and 466.0 eV ascribed to Ru^{3+}, Ru^{4+} and a shake-up satellite peak, respectively [71–73]. As expected, Ru^{4+} cations are the predominant Ru species in $NdMn_{1.5}Ru_{0.5}O_5$. The small fraction of Ru^{3+} detected by XPS is in line with the content of Ru^{3+} of approximately 5% in the phase as determined from the refinement of the crystal structure of $NdMn_{1.5}Ru_{0.5}O_5$ (see Fig. 1), which is also in line with previous reports [47]. The Mn $2p_{3/2}$ core-level region (see Fig. S4b) was fitted into two components, with peak maxima at 641.6 and 642.6 eV and ascribed to Mn^{3+} and Mn^{4+}, respectively [74–76]. The Mn^{4+}/Mn^{3+} ratio changes slightly from 1.12 in the initial catalyst to 0.9 after 500 OER cycles, and to 0.64 after 1000 cycles, indicating a slight reduction of the oxidation state of Mn cations at the surface after the cycles. The Nd $3d_{5/2}$ region (Fig. S4c) has three components [77–79], a peak at 982.3 eV ascribed to Nd^{3+}, an Auger feature (O KLL) at 973.4 eV, and a satellite line at 978.6 eV due to the electron transfer from the oxygen ligand to the Nd 4*f* [77,80]. Moreover, the peak spin-orbit splitting of 22.6 eV between the Nd $3d_{5/2}$ and Nd $3d_{3/2}$ peaks confirms the presence of Nd^{3+} [79]. In fact, the Nd region intensity has significantly decreased after 1000 OER cycles, making it challenging to identify accurately the components. Nevertheless, the binding energy of the peak is not affected after cycling, confirming that the oxidation state of Nd^{3+} remains constant during the OER.

As shown in Fig. S5, neither the position nor the shape of the Ru $3p_{3/2}$, Mn $2p_{3/2}$, and Nd $3d_{5/2}$ peaks varies significantly during the OER; only a slight change in Mn oxidation state can be observed. These results suggest that the nature of the surface species remains stable during the OER. The surface atomic composition of the fresh and of the catalyst recovered after OER was determined from the area of the XPS peaks normalized by the corresponding sensitivity factors [72]. As shown in Fig. 3c (see also Tables S4 and SI), the Ru/Mn surface atomic ratio of the fresh sample, 0.55, is slightly higher than the stoichiometric ratio of 0.33, indicating a slight surface Ru-enrichment on the fresh catalyst. After the first OER cycles, the surface Ru-enrichment is even more evident, which is consistent with the increase in the OER activity during the first 200 cycles and supports previous observations that Ru is the main active site for the OER [28,60]. Also, the hypothesis of Ru sites being the main active sites is supported by the fact that the compound $NdMn_2O_5$ presents significantly lower OER activity in acidic media than the Ru-containing sample ($NdMn_{1.5}Ru_{0.5}O_5$) when measured under the same reaction conditions, see Fig. S6 in the SI. This observation leads to the conclusion that the OER activity is mainly influenced by the presence of Ru cations in the catalyst. However, the influence of Mn cannot be disregarded. Previous studies from our group demonstrated that the presence of Mn promotes the OER activity in R_2MnRuO_7 due to the formation of Ru-O-Mn surface ensembles [34,66], so the presence of both Mn and Ru in the $(Mn,Ru)^{4+}O_6$ octahedra in $NdMn_{1.5}Ru_{0.5}O_5$ is also expected to promote its high OER activity. The Ru/Mn surface atomic ratio of the catalyst remains elevated even after 500 and 1000 OER cycles, higher than the stoichiometric ratio of 0.55 of the starting material. However, it consistently decreases over cycling, which can explain in part the decrease in activity between 500 and 1000 OER cycles.

The evolution of the bulk composition of $NdMn_{1.5}Ru_{0.5}O_5$ during the OER has been studied with EDS. After 500 OER cycles, a small loss of Ru is observed, resulting in an oxide with a stoichiometry of $NdMn_{1.4}Ru_{0.3}O_x$. Considering that the activity starts decaying after 200 cycles, this observation suggests again that Ru atoms are the dominant active sites for the OER. A very similar stoichiometry is found after 1000 OER, only with a slightly higher loss of Mn to 1.32 atomic content. It is important to clarify that, despite these compositional variations during the OER, the bulk crystal structure of $NdMn_{1.5}Ru_{0.5}O_5$ remains stable during the stability test, as demonstrated by the x-ray diffractograms of the fresh and used catalysts (Fig. 3b).

The evolution of the catalyst's morphology and structure during the OER has been analyzed with TEM. Fig. 4 displays representative TEM images of the fresh and spent catalyst after 500 OER cycles. The particles of the fresh catalyst (Fig. 4a, b, and c) display a dense morphology and relatively large size with a heterogeneous particle size distribution, around 50–200 nm (mean particle size of 139 ± 25 nm. After 500 OER cycles, TEM images fail to reveal any evidence of amorphization or formation of new phases (Fig. 4d). The HRTEM image (Fig. 4e) shows that the crystal structure of $NdMn_{1.5}Ru_{0.5}O_5$ remains stable during the OER. However, a careful inspection of the TEM micrographs of the catalyst recovered after 500 OER cycles reveals that a small number of particles display an incipient degradation of their surface due to partial dissolution of the oxide (Fig. 4f). Also, the mean particle size decreases slightly to 118 ± 30 nm after 500 cycles.

A TEM analysis was conducted on the catalyst recovered after 1000

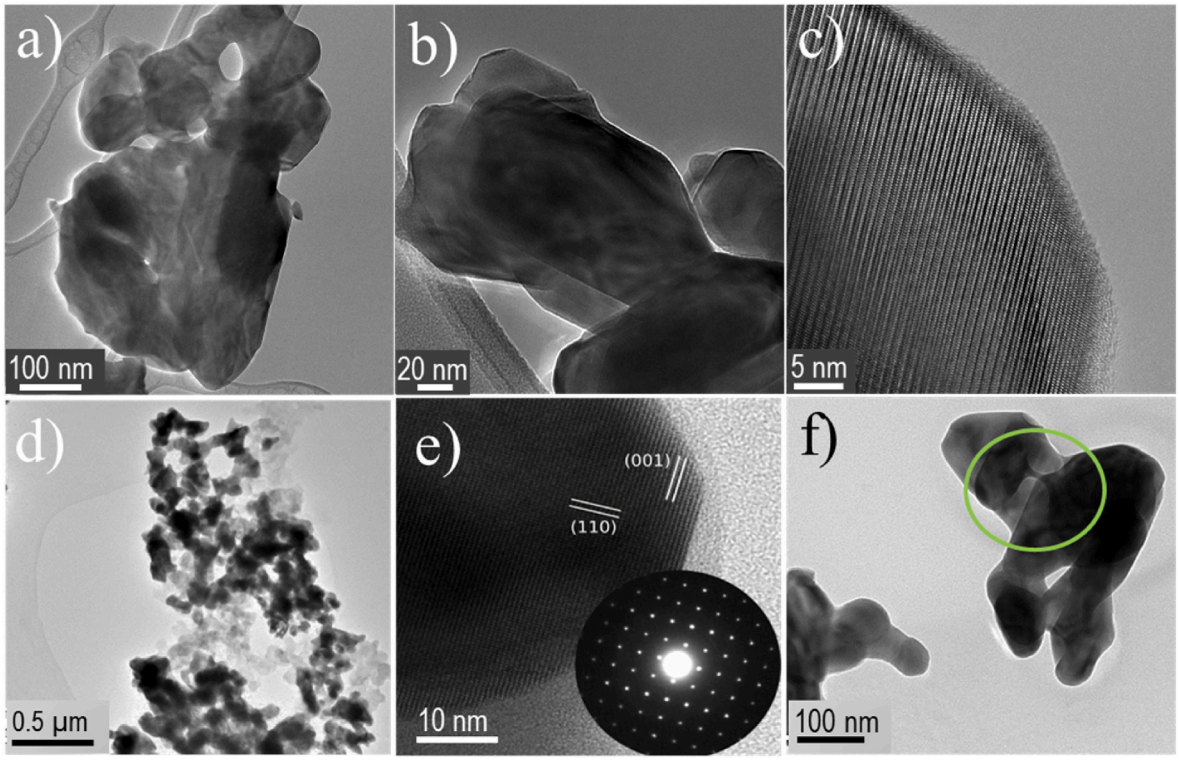

Fig. 4. (a, b) TEM micrographs of $NdMn_{1.5}Ru_{0.5}O_5$ fresh catalyst. (c) HRTEM of the fresh catalyst. (d) TEM micrographs of the catalyst after 500 OER cycles. (e) HRTEM image of a $NdMn_{1.5}Ru_{0.5}O_5$ crystal oriented down the [−110] direction of the orthorhombic structure of the catalyst after 500 OER cycles. Inset of Fig. 4e: diffraction pattern oriented with respect to the image. (f) TEM micrograph of $NdMn_{1.5}Ru_{0.5}O_5$ after 500 cycles.

OER cycles. A significant reduction in particle size was observed, as shown in Fig. 5a, with a mean particle size of 80 ± 20 nm. Furthermore, the particles exhibited slightly less aggregation and displayed a distinct bar-like morphology. However, electron diffraction analysis is consistent with the presence of the $NdMn_{1.5}Ru_{0.5}O_5$ crystal structure, as illustrated in Fig. 5b. Fig. 5c and d depict representative TEM images illustrating the catalyst's degradation. Fig. 5d shows the incipient degradation of $NdMn_{1.5}Ru_{0.5}O_5$, featuring particles with holes similar to those observed already after 500 OER cycles. Fig. 5c shows the presence of large particles along with areas composed of nanosized particles (see the inset to Fig. 5c). Unfortunately, the composition of these particles could not be determined from EDS analysis due to the prominent intensity of the Cu signal arising from the TEM grid, but it is worth noting that they are only observed after the OER activity of the catalyst declines after 1000 cycles.

The analysis of cation release into the electrolyte during the OER was

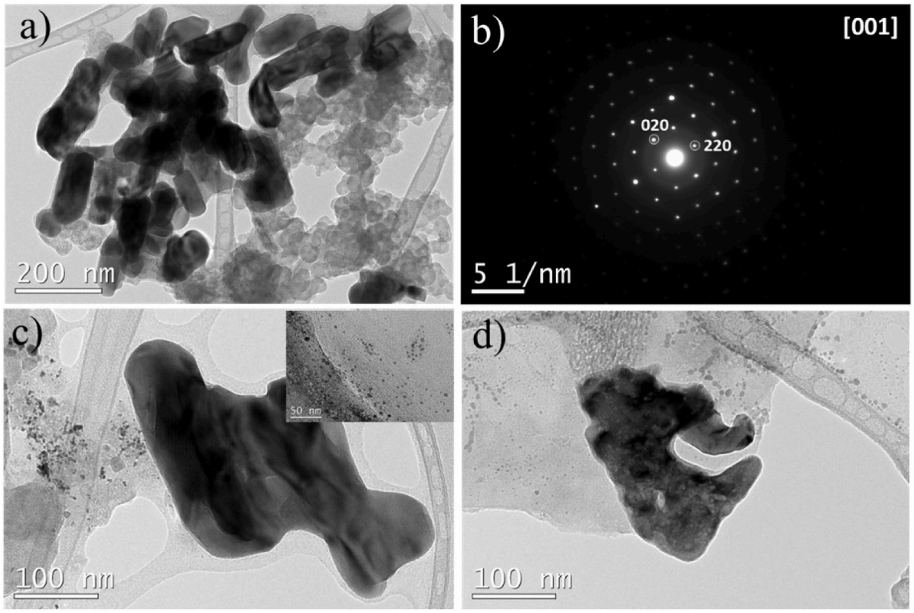

Fig. 5. TEM characterization of $NdMn_{1.5}Ru_{0.5}O_5$ after 1000 OER cycles: (a) Representative TEM image of a set of particles. (b) SAED of one particle along the [001] zone axis of the initial structure. (c) TEM micrograph showing the appearance of nanoparticles (inset). (d) TEM micrograph of a more degraded particle.

conducted using ICP. Electrolyte samples were extracted following 500 and 1000 OER cycles carried out between 1.2 and 1.7 V at 10 mVs^{-1} in O_2-saturated 0.1 M $HClO_4$, utilizing 2.5 mg of catalyst deposited onto carbon paper. After 500 cycles, there was a mass reduction of 0.71%, 1.21%, and 1.5% for Ru, Mn, and Nd, respectively. This loss became more pronounced after 1000 cycles, with values escalating to 3.9%, 21.6%, and 31% for Ru, Mn, and Nd, respectively. Therefore, the reduction in particle size observed in TEM images can be attributed to the dissolution of approximately one-third of Mn and Nd cations from the catalyst. This phenomenon results in material loss over cycling, thereby contributing to the observed decrease in activity. Notably, only around 4% of Ru is dissolved into the electrolyte during the OER. This observation is in conflict with the observation (XRD and electron diffraction) that the crystal structure of the large particles is the same as that of the initial sample, $NdMn_{1.5}Ru_{0.5}O_5$, as corroborated also by EDS. In view of these observations, it is plausible that the nanoparticles observed by TEM in the catalyst recovered after 1000 OER cycles are primarily Ru-based particles. While these nanosized Ru-based nanoparticles would probably retain some level of activity, the Ru–Mn-rich surface found in the $NdMn_{1.5}Ru_{0.5}O_5$ particles is responsible for the high OER activity.

3.5. PEMWE measurements

The $NdMn_{1.5}Ru_{0.5}O_5$ catalyst is used to produce a PEMWE anode with a loading of 0.5 mg_{Ru} cm^{-2} and subsequently tested in a single cell with an active area of 4 cm^2. Fig. 6a shows the polarization curve recorded up to 0.5 A cm^{-2} at 80 °C and 1 bar. The PEMWE with $NdMn_{1.5}Ru_{0.5}O_5$ anode achieves 1.97 V at 0.5 A cm^{-2}. Although the activity test reported in this work has been performed with one order of magnitude less Ru loading than the usual Ru anodes [81,82], the performance achieved by our PEMWE cell lies within the state-of-the-art Ru-based catalysts. Comparing the performance of the PEMWE described in our work with the literature is not straightforward as the performance PEMWEs depends not only on the catalysts but on multiple factors. These factors include the components of the PEMWE (membrane and the PTLs) and operational parameters such as pressure, temperature, and catalyst loading. As observed in Table S5, our PEMWE displays a similar performance to other PEMWE cells reported in the literature measured in similar conditions. However, it is crucial to remark that the Ru loading of 0.5 mg used in our cell is significantly lower than that used in previous studies, ranging between 2 and 3 mg_{Ru} cm^{-2}.

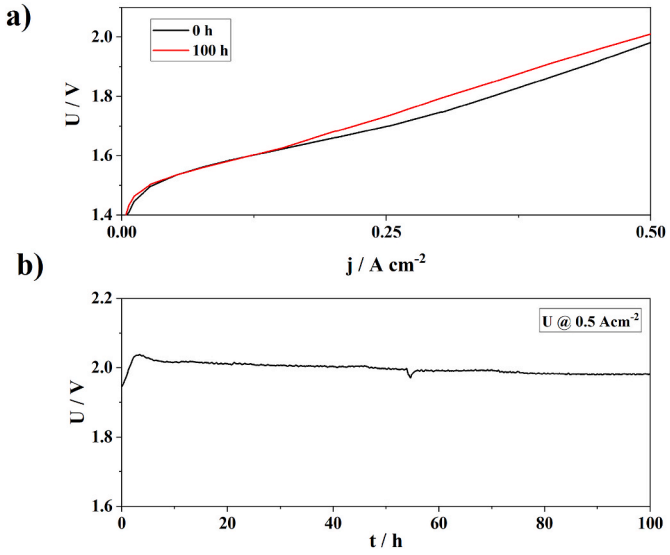

Fig. 6. a) Polarization curve up to 0.5 A cm^{-2} before (black) and after (red) and b) cell potential at a constant current density of 0.5 A cm^{-2} during 100 h for a PEMWE based in 0.4 mg_{Pt} cm^{-2} as cathode and 0.5 mg_{Ru} cm^{-2} as anode obtained at 80 °C and 1 bar with Nafion 212 membrane. (For interpretation of the references to colour in this figure legend, the reader is referred to the Web version of this article.)

However, the major problem with Ru-based catalysts is their durability, especially when measuring at current densities above 0.2 A cm^{-2} [83], especially for Ir-free Ru-based catalysts [14]. To assess the durability of the CCM, we conducted durability tests at a constant current density of 0.5 A cm^{-2} during 100 h, see Fig. 6. Note that this current density is higher than those usually reported in the literature for the measurement of the catalytic activity of Ru-based catalysts in PEMWE, usually ranging between approximately 0.1–0.2 A cm^{-2}. The initial polarization curve and the one obtained after 100 h of durability test are depicted in Fig. 6a. As observed, the cell potential needed to maintain a current density of 0.5 A cm^{-2} increases after 100 h of operation. On the other hand, the durability test shown in Fig. 6b shows the opposite trend, that is, a slight decreasing in voltage during operation. However, Fig. 6b shows a rapid increase of the potential in the first 3 h of operation, which does not normally occur in the case of Ir-based anodes. The activation process of Ir typically leads to a decrease in the cell potential in the initial hours of operation of the PEMWE until it remains constant or, in some cases, starts to increase at a rate of a few μV h^{-1}. However, in the case $NdMn_{1.5}Ru_{0.5}O_5$, it seems that the material structure or surface changes in the first 3 h of operation, but then it stabilizes. This is a remarkable behavior for a Ru-based catalyst, especially considering its low Ru loading. Moreover, at around 53 h, a shutdown was carried out. Impressively, the cell recovers its performance almost immediately, indicating the high stability of $NdMn_{1.5}Ru_{0.5}O_5$. Thus, the results obtained in PEMWE position $NdMn_{1.5}Ru_{0.5}O_5$ as a potential stable catalyst candidate for PEMWE anodes based on Ru with low loadings.

4. Conclusions

$NdMn_{1.5}Ru_{0.5}O_5$, a Ru-mixed oxide with the structure of the $DyMn_2O_5$ family, displays high OER performance in acidic media. Its OER activity can be ascribed to the presence of Ru^{4+} cations in octahedra sites with short Ru–Ru distances between octahedra, along with the presence of Mn and Ru cations. $NdMn_{1.5}Ru_{0.5}O_5$ exhibits good durability for the OER, maintaining its activity for several hundreds of cycles while preserving its bulk crystal structure. Surface Ru enrichment is observed even in the fresh catalyst and increases during the first hundred of cycles, contributing to the high activity of the material. After 1000 OER cycles, cation leaching into the electrolyte becomes more pronounced, particularly for Mn and Nd, leading to a decline in catalytic activity. The catalyst was tested in a PEMWE, showing high stability during 100 h of operation at 0.5 A cm^{-2}. While the cell performance is lower compared to those obtained with Ir-based catalysts, it compares favorably with state-of-the-art PEMWE cells featuring low-loaded Ru anodes. Notably, the high stability of the cell during operation represents a significant advancement for Ru-based catalysts in PEMWE. Lastly, in addition to the high OER activity, $NdMn_{1.5}Ru_{0.5}O_5$ also demonstrates the rare capability to be active for ORR, thus rendering a bifunctional electrocatalyst. Thus, besides its application in PEMWE, the material holds potential for use in unitized regenerative fuel cell and batteries.

CRediT authorship contribution statement

Isabel Rodríguez-García: Investigation, Formal analysis. **José Luis Gómez de la Fuente:** Investigation, Formal analysis. **Jorge Torrero:** Investigation. **Daniel García Sánchez:** Supervision, Investigation. **Mohamed Abdel Salam:** Investigation, Funding acquisition. **José Antonio Alonso:** Investigation. **Aldo Saul Gago:** Supervision, Investigation. **Kaspar Andreas Friedrich:** Supervision. **Sergio Rojas:** Writing – review & editing, Writing – original draft, Supervision, Methodology, Funding acquisition, Formal analysis, Conceptualization. **María**

Retuerto: Writing – original draft, Supervision, Methodology, Investigation, Funding acquisition, Formal analysis. **Álvaro Tolosana-Moranchel:** Writing – original draft, Investigation, Formal analysis.

Declaration of competing interest

The authors declare that they have no known competing financial interests or personal relationships that could have appeared to influence the work reported in this paper.

Data availability

Data will be made available on request.

Acknowledgements

This work was funded by PROMET-H2 project from the European Union's Horizon 2020 research and innovation programme under grant agreement No 862253; also, by the Deputyship for Research & Innovation, Ministry of Education of Saudi Arabia for the project number 341; and by the Spanish grants PID2020-116712RB-C21, PID2021-122477OB-I00 and TED2021-131033B–I00 from MCIN/AEI/10.13039/501100011033. A. T-M thanks the Consejería de Educación, Juventud y Deporte of the Comunidad de Madrid for the Ayuda Destinada a la Atracción de Talento Investigador (2020-T2/AMB-19927). I. R-G thanks the PhD Program in Electroquímica, Ciencia y Tecnología of Escuela de doctorado of Universidad Autónoma de Madrid.

Appendix A. Supplementary data

Supplementary data to this article can be found online at https://doi.org/10.1016/j.jpowsour.2024.234416.

References

[1] M. Chatenet, B.G. Pollet, D.R. Dekel, F. Dionigi, J. Deseure, P. Millet, R.D. Braatz, M.Z. Bazant, M. Eikerling, I. Staffell, P. Balcombe, Y. Shao-Horn, H. Schäfer, Water electrolysis: from textbook knowledge to the latest scientific strategies and industrial developments, Chem. Soc. Rev. 51 (2022) 4583–4762, https://doi.org/10.1039/D0CS01079K.

[2] IRENA, Green hydrogen cost reduction, Scaling up Electrolysers to Meet the 1.5°C Climate Goal, 2020. https://www.irena.org/-/media/Files/IRENA/Agency/Publication/2020/Dec/IRENA_Green_hydrogen_cost_2020.pdf. (Accessed 11 February 2021).

[3] A. Weiß, A. Siebel, M. Bernt, T.-H. Shen, V. Tileli, H.A. Gasteiger, Impact of Intermittent operation on lifetime and performance of a PEM water electrolyzer, J. Electrochem. Soc. 166 (2019) F487–F497, https://doi.org/10.1149/2.0421908jes.

[4] D. Galyamin, Á. Tolosana-Moranchel, M. Retuerto, S. Rojas, Unraveling the most relevant features for the design of iridium mixed oxides with high activity and durability for the oxygen evolution reaction in acidic media, JACS Au 3 (2023) 2336–2355, https://doi.org/10.1021/jacsau.3c00247.

[5] Johnson Matthey, PGM market report, PGM Mark. Rep (2021) 1–48. May 2021.

[6] M. Bernt, A. Hartig-Weiß, M.F. Tovini, H.A. El-Sayed, C. Schramm, J. Schröter, C. Gebauer, H.A. Gasteiger, Current challenges in catalyst development for PEM water electrolyzers, Chem.-Ing.-Tech. 92 (2020) 31–39, https://doi.org/10.1002/CITE.201900101.

[7] M. Clapp, C.M. Zalitis, M. Ryan, Perspectives on current and future iridium demand and iridium oxide catalysts for PEM water electrolysis, Catal. Today 420 (2023) 114140, https://doi.org/10.1016/j.cattod.2023.114140.

[8] J. Torrero, T. Morawietz, D. García Sanchez, D. Galyamin, M. Retuerto, V. Martin-Diaconescu, S. Rojas, J.A. Alonso, A.S. Gago, K.A. Friedrich, High performance and durable anode with 10-fold reduction of iridium loading for proton exchange membrane water electrolysis, Adv. Energy Mater. 13 (2023) 2204169, https://doi.org/10.1002/aenm.202204169.

[9] M. Retuerto, L. Pascual, J. Torrero, M.A. Salam, Á. Tolosana-Moranchel, D. Gianolio, P. Ferrer, P. Kayser, V. Wilke, S. Stiber, V. Celorrio, M. Mokthar, D. G. Sanchez, A.S. Gago, K.A. Friedrich, M.A. Peña, J.A. Alonso, S. Rojas, Highly active and stable OER electrocatalysts derived from Sr2MIrO6 for proton exchange membrane water electrolyzers, Nat. Commun. 13 (2022) 7935, https://doi.org/10.1038/s41467-022-35631-5.

[10] T. Lickert, S. Fischer, J.L. Young, S. Klose, I. Franzetti, D. Hahn, Z. Kang, M. Shviro, F. Scheepers, M. Carmo, T. Smolinka, G. Bender, S. Metz, Advances in benchmarking and round robin testing for PEM water electrolysis: reference protocol and hardware, Appl. Energy 352 (2023) 121898, https://doi.org/10.1016/j.apenergy.2023.121898.

[11] F. Zhou, L. Zhang, J. Li, Q. Wang, Y. Chen, H. Chen, G. Lu, G. Chen, H. Jin, S. Wang, J. Wang, Novel engineering of ruthenium-based electrocatalysts for acidic water oxidation: a mini review, Eng. Reports. 3 (2021) 1–22, https://doi.org/10.1002/eng2.12437.

[12] S.H. Chang, N. Danilovic, K.C. Chang, R. Subbaraman, A.P. Paulikas, D.D. Fong, M. J. Highland, P.M. Baldo, V.R. Stamenkovic, J.W. Freeland, J.A. Eastman, N. M. Markovic, Functional links between stability and reactivity of strontium ruthenate single crystals during oxygen evolution, Nat. Commun. 5 (2014) 4191, https://doi.org/10.1038/ncomms5191.

[13] B.-J. Kim, D.F. Abbott, X. Cheng, E. Fabbri, M. Nachtegaal, F. Bozza, I.E. Castelli, D. Lebedev, R. Schäublin, C. Copéret, T. Graule, N. Marzari, T.J. Schmidt, Unraveling thermodynamics, stability, and oxygen evolution activity of strontium ruthenium perovskite oxide, ACS Catal. 7 (2017) 3245–3256, https://doi.org/10.1021/acscatal.6b03171.

[14] V.A. Saveleva, L. Wang, W. Luo, S. Zafeiratos, C. Ulhaq-Bouillet, A.S. Gago, K. A. Friedrich, E.R. Savinova, Uncovering the stabilization mechanism in bimetallic ruthenium–iridium anodes for proton exchange membrane electrolyzers, J. Phys. Chem. Lett. 7 (2016) 3240–3245, https://doi.org/10.1021/acs.jpclett.6b01500.

[15] S. Laha, Y. Lee, F. Podjaski, D. Weber, V. Duppel, L.M. Schoop, F. Pielnhofer, C. Scheurer, K. Müller, U. Starke, K. Reuter, B. V Lotsch, Ruthenium oxide nanosheets for enhanced oxygen evolution catalysis in acidic medium, Adv. Energy Mater. 9 (2019) 1–8, https://doi.org/10.1002/aenm.201803795.

[16] Z.L. Zhao, Q. Wang, X. Huang, Q. Feng, S. Gu, Z. Zhang, H. Xu, L. Zeng, M. Gu, H. Li, Boosting the oxygen evolution reaction using defect-rich ultra-thin ruthenium oxide nanosheets in acidic media, Energy Environ. Sci. 13 (2020) 5143–5151, https://doi.org/10.1039/d0ee01960g.

[17] Y. Yao, S. Hu, W. Chen, Z.-Q. Huang, W. Wei, T. Yao, R. Liu, K. Zang, X. Wang, G. Wu, W. Yuan, T. Yuan, B. Zhu, W. Liu, Z. Li, D. He, Z. Xue, Y. Wang, X. Zheng, J. Dong, C.-R. Chang, Y. Chen, X. Hong, J. Luo, S. Wei, W.-X. Li, P. Strasser, Y. Wu, Y. Li, Engineering the electronic structure of single atom Ru sites via compressive strain boosts acidic water oxidation electrocatalysis, Nat. Catal. 2 (2019) 304–313, https://doi.org/10.1038/s41929-019-0246-2.

[18] Z. Shi, J. Li, Y. Wang, S. Liu, J. Zhu, J. Yang, X. Wang, J. Ni, Z. Jiang, L. Zhang, Y. Wang, C. Liu, W. Xing, J. Ge, Customized reaction route for ruthenium oxide towards stabilized water oxidation in high-performance PEM electrolyzers, Nat. Commun. 14 (2023) 843, https://doi.org/10.1038/s41467-023-36380-9.

[19] Y. Lin, Z. Tian, L. Zhang, J. Ma, Z. Jiang, B.J. Deibert, R. Ge, L. Chen, Chromium-ruthenium oxide solid solution electrocatalyst for highly efficient oxygen evolution reaction in acidic media, Nat. Commun. 10 (2019) 162, https://doi.org/10.1038/s41467-018-08144-3.

[20] S. Hao, M. Liu, J. Pan, X. Liu, X. Tan, N. Xu, Y. He, L. Lei, X. Zhang, Dopants fixation of Ruthenium for boosting acidic oxygen evolution stability and activity, Nat. Commun. 11 (2020) 5368, https://doi.org/10.1038/s41467-020-19212-y.

[21] J. Wang, Y. Ji, R. Yin, Y. Li, Q. Shao, X. Huang, Transition metal-doped ultrathin RuO2 networked nanowires for efficient overall water splitting across a broad pH range, J. Mater. Chem. A. 7 (2019) 6411–6416, https://doi.org/10.1039/c9ta00598f.

[22] J. Su, R. Ge, K. Jiang, Y. Dong, F. Hao, Z. Tian, G. Chen, L. Chen, Assembling ultrasmall copper-doped ruthenium oxide nanocrystals into hollow porous polyhedra: highly robust electrocatalysts for oxygen evolution in acidic media, Adv. Mater. 30 (2018) 1–8, https://doi.org/10.1002/adma.201801351.

[23] L. Li, G. Zhang, J. Xu, H. He, B. Wang, Z. Yang, S. Yang, Optimizing the electronic structure of ruthenium oxide by neodymium doping for enhanced acidic oxygen evolution catalysis, Adv. Funct. Mater. 33 (2023), https://doi.org/10.1002/adfm.202213304.

[24] C. Lin, J.-L. Li, X. Li, S. Yang, W. Luo, Y. Zhang, S.-H. Kim, D.-H. Kim, S.S. Shinde, Y.-F. Li, Z.-P. Liu, Z. Jiang, J.-H. Lee, In-situ reconstructed Ru atom array on α-MnO2 with enhanced performance for acidic water oxidation, Nat. Catal. 4 (2021) 1012–1023, https://doi.org/10.1038/s41929-021-00703-0.

[25] S.H. Chang, J.G. Connell, N. Danilovic, R. Subbaraman, K.C. Chang, V. R. Stamenkovic, N.M. Markovic, Activity-stability relationship in the surface electrochemistry of the oxygen evolution reaction, Faraday Discuss 176 (2014) 125–133, https://doi.org/10.1039/c4fd00134f.

[26] M. Retuerto, L. Pascual, F. Calle-Vallejo, P. Ferrer, D. Gianolio, A.G. Pereira, Á. García, J. Torrero, M.T. Fernández-Díaz, P. Bencok, M.A. Peña, J.L.G. Fierro, S. Rojas, Na-doped ruthenium perovskite electrocatalysts with improved oxygen evolution activity and durability in acidic media, Nat. Commun. 10 (2019) 2041, https://doi.org/10.1038/s41467-019-09791-w.

[27] I. Rodríguez-García, D. Galyamin, L. Pascual, P. Ferrer, M.A. Peña, D. Grinter, G. Held, M. Abdel Salam, M. Mokhtar, K. Narasimharao, M. Retuerto, S. Rojas, Enhanced stability of SrRuO3 mixed oxide via monovalent doping in Sr1-xKxRuO3 for the oxygen evolution reaction, J. Power Sources 521 (2022) 230950, https://doi.org/10.1016/j.jpowsour.2021.230950.

[28] X. Miao, L. Zhang, L. Wu, Z. Hu, L. Shi, S. Zhou, Quadruple perovskite ruthenate as a highly efficient catalyst for acidic water oxidation, Nat. Commun. 10 (2019) 1–7, https://doi.org/10.1038/s41467-019-11789-3.

[29] M.A. Hubert, A.M. Patel, A. Gallo, Y. Liu, E. Valle, M. Ben-Naim, J. Sanchez, D. Sokaras, R. Sinclair, J.K. Nørskov, L.A. King, M. Bajdich, T.F. Jaramillo, Acidic oxygen evolution reaction activity-stability relationships in Ru-based pyrochlores, ACS Catal. 10 (2020) 12182–12196, https://doi.org/10.1021/acscatal.0c02252.

[30] M. Kim, J. Park, M. Kang, J.Y. Kim, S.W. Lee, Toward efficient electrocatalytic oxygen evolution: emerging opportunities with metallic pyrochlore oxides for electrocatalysts and conductive supports, ACS Cent. Sci. 6 (2020) 880–891, https://doi.org/10.1021/acscentsci.0c00479.

[31] C. Zhang, F. Wang, B. Xiong, H. Yang, Regulating the electronic structures of mixed B-site pyrochlore to enhance the turnover frequency in water oxidation, Nano Converg 9 (2022), https://doi.org/10.1186/s40580-022-00311-z.
[32] J. Kim, P.C. Shih, K.C. Tsao, Y.T. Pan, X. Yin, C.J. Sun, H. Yang, High-performance pyrochlore-type yttrium ruthenate electrocatalyst for oxygen evolution reaction in acidic media, J. Am. Chem. Soc. 139 (2017) 12076–12083, https://doi.org/10.1021/jacs.7b06808.
[33] Q. Feng, Q. Wang, Z. Zhang, Y. Xiong, H. Li, Y. Yao, X.Z. Yuan, M.C. Williams, M. Gu, H. Chen, H. Li, H. Wang, Highly active and stable ruthenate pyrochlore for enhanced oxygen evolution reaction in acidic medium electrolysis, Appl. Catal. B Environ. 244 (2019) 494–501, https://doi.org/10.1016/j.apcatb.2018.11.071.
[34] D. Galyamin, J. Torrero, I. Rodríguez, M.J. Kolb, P. Ferrer, L. Pascual, M.A. Salam, D. Gianolio, V. Celorrio, M. Mokhtar, D. Garcia Sanchez, A.S. Gago, K.A. Friedrich, M.A. Peña, J.A. Alonso, F. Calle-Vallejo, M. Retuerto, S. Rojas, Active and durable R2MnRuO7 pyrochlores with low Ru content for acidic oxygen evolution, Nat. Commun. 14 (2023) 2010, https://doi.org/10.1038/s41467-023-37665-9.
[35] N. Zhang, C. Wang, J. Chen, C. Hu, J. Ma, X. Deng, B. Qiu, L. Cai, Y. Xiong, Y. Chai, Metal substitution steering electron correlations in pyrochlore ruthenates for efficient acidic water oxidation, ACS Nano 15 (2021) 8537–8548, https://doi.org/10.1021/acsnano.1c00266.
[36] H. Liu, Z. Wang, M. Li, X. Zhao, X. Duan, S. Wang, G. Tan, Y. Kuang, X. Sun, Rare-earth-regulated Ru-O interaction within the pyrochlore ruthenate for electrocatalytic oxygen evolution in acidic media, Sci. China Mater. 64 (2021) 1653–1661, https://doi.org/10.1007/s40843-020-1571-y.
[37] Y. Lin, Y. Dong, X. Wang, L. Chen, Electrocatalysts for the oxygen evolution reaction in acidic media, Adv. Mater. 35 (2023), https://doi.org/10.1002/adma.202210565.
[38] A. Li, S. Kong, C. Guo, H. Ooka, K. Adachi, D. Hashizume, Q. Jiang, H. Han, J. Xiao, R. Nakamura, Enhancing the stability of cobalt spinel oxide towards sustainable oxygen evolution in acid, Nat. Catal. 5 (2022) 109–118, https://doi.org/10.1038/s41929-021-00732-9.
[39] M. Chatti, J.L. Gardiner, M. Fournier, B. Johannessen, T. Williams, T. R. Gengenbach, N. Pai, C. Nguyen, D.R. MacFarlane, R.K. Hocking, A.N. Simonov, Intrinsically stable in situ generated electrocatalyst for long-term oxidation of acidic water at up to 80 °C, Nat. Catal. 2 (2019) 457–465, https://doi.org/10.1038/s41929-019-0277-8.
[40] S. Pan, H. Li, D. Liu, R. Huang, X. Pan, D. Ren, J. Li, M. Shakouri, Q. Zhang, M. Wang, C. Wei, L. Mai, B. Zhang, Y. Zhao, Z. Wang, M. Graetzel, X. Zhang, Efficient and stable noble-metal-free catalyst for acidic water oxidation, Nat. Commun. 13 (2022) 2294, https://doi.org/10.1038/s41467-022-30064-6.
[41] M. Chisaka, H. Morioka, Phosphor and nitrogen co-doped rutile TiO 2 covered on TiN for oxygen reduction reaction in acidic media, Catal. Sci. Technol. 9 (2019) 611–619, https://doi.org/10.1039/c8cy01973h.
[42] A. Ishihara, M. Arao, M. Matsumoto, T. Tokai, T. Nagai, Y. Kuroda, K. Matsuzawa, H. Imai, S. Mitsushima, K. ichiro Ota, Niobium-added titanium oxides powders as non-noble metal cathodes for polymer electrolyte fuel cells – electrochemical evaluation and effect of added amount of niobium, Int. J. Hydrogen Energy 45 (2020) 5438–5448, https://doi.org/10.1016/j.ijhydene.2019.08.217.
[43] A. Ishihara, Y. Yamamoto, O. Sugino, K. Ota, Oxygen reduction reaction (ORR) in acidic media with nanostructured metal oxide-based electrocatalysts, in: Met. Oxide-Based Nanostructured Electrocatal. Fuel Cells, Electrolyzers, Met. Batter., Elsevier, 2021, pp. 37–59, https://doi.org/10.1016/B978-0-12-818496-7.00006-0.
[44] A. Ishihara, T. Nagai, K. Ukita, M. Arao, M. Matsumoto, L. Yu, T. Nakamura, O. Sekizawa, Y. Takagi, K. Matsuzawa, T.W. Napporn, S. Mitsushima, T. Uruga, T. Yokoyama, Y. Iwasawa, H. Imai, K.I. Ota, Emergence of oxygen reduction activity in zirconium oxide-based compounds in acidic media: creation of active sites for the oxygen reduction reaction, J. Phys. Chem. C 123 (2019) 18150–18159, https://doi.org/10.1021/acs.jpcc.9b02393.
[45] P.P. Patel, M.K. Datta, O.I. Velikokhatnyi, R. Kuruba, K. Damodaran, P. Jampani, B. Gattu, P.M. Shanthi, S.S. Damle, P.N. Kumta, Noble metal-free bifunctional oxygen evolution and oxygen reduction acidic media electro-catalysts, Sci. Rep. 6 (2016) 1–14, https://doi.org/10.1038/srep28367.
[46] V. Rai, K.P. Lee, D. Safanama, S. Adams, D.J. Blackwood, Oxygen reduction and evolution reaction (ORR and OER) bifunctional electrocatalyst operating in a wide pH range for cathodic application in Li–air batteries, ACS Appl. Energy Mater. 3 (2020) 9417–9427, https://doi.org/10.1021/acsaem.0c01775.
[47] C. de la Calle, J.A. Alonso, M.J. Martínez-Lope, M. Retuerto, M. García-Hernández, M.T. Fernández-Díaz, Ru–Ru metal–metal bonding in the chains of edge-sharing octahedra of NdMn 1.5 Ru 0.5 O 5 : a Neutron powder diffraction and magnetic study, Eur. J. Inorg. Chem. 2010 (2010) 781–789, https://doi.org/10.1002/ejic.200900626.
[48] H.M. Rietveld, A profile refinement method for nuclear and magnetic structures, J. Appl. Crystallogr. 2 (1969) 65–71, https://doi.org/10.1107/S0021889869006558.
[49] J. Rodríguez-carvajal, Recent developments of the program FULLPROF, Int. Union Crystallogr. Newsl 2 (2001) 12–19. December, https://www.fkf.mpg.de/4112052/cpd26.pdf.
[50] S. Stiber, H. Balzer, A. Wierhake, F.J. Wirkert, J. Roth, U. Rost, M. Brodmann, J. K. Lee, A. Bazylak, W. Waiblinger, A.S. Gago, K.A. Friedrich, Porous transport layers for proton exchange membrane electrolysis under extreme conditions of current density, temperature, and pressure, Adv. Energy Mater. 11 (2021) 2100630, https://doi.org/10.1002/aenm.202100630.
[51] T. Malkow, A. Pilenga, G. Tsotridis, EU harmonised polarisation curve test method for low temperature water electrolysis. https://doi.org/10.2760/179509, 2018.
[52] S.C. Abrahams, J.L. Bernstein, Crystal structure of paramagnetic DyMn2O5 at 298°K, J. Chem. Phys. 46 (1967) 3776–3782, https://doi.org/10.1063/1.1840450.
[53] A. V Morozkin, Y.D. Seropegin, Sm–Ru–Ge system at 1070 K, J. Alloys Compd. 365 (2004) 168–172, https://doi.org/10.1016/S0925-8388(03)00652-2.
[54] D. Huang, S. Liu, H. Xu, Y. Du, Phase equilibria of the Mg–Mn–Zn system at 593 K (320 °C), J. Alloys Compd. 688 (2016) 1115–1124, https://doi.org/10.1016/j.jallcom.2016.07.120.
[55] C.C.L. McCrory, S. Jung, J.C. Peters, T.F. Jaramillo, Benchmarking heterogeneous electrocatalysts for the oxygen evolution reaction, J. Am. Chem. Soc. 135 (2013) 16977–16987, https://doi.org/10.1021/ja407115p.
[56] J. Kim, P. Shih, Y. Qin, Z. Al-Bardan, C. Sun, H. Yang, A porous pyrochlore Y 2 [Ru 1.6 Y 0.4]O 7– δ electrocatalyst for enhanced performance towards the oxygen evolution reaction in acidic media, Angew. Chemie Int. Ed. 57 (2018) 13877–13881, https://doi.org/10.1002/anie.201808825.
[57] X. Wu, C. Tang, Y. Cheng, X. Min, S.P. Jiang, S. Wang, Bifunctional catalysts for reversible oxygen evolution reaction and oxygen reduction reaction, Chem. Eur J. 26 (2020) 3906–3929, https://doi.org/10.1002/chem.201905346.
[58] G. Chen, S.R. Bare, T.E. Mallouk, Development of supported bifunctional electrocatalysts for unitized regenerative fuel cells, J. Electrochem. Soc. 149 (2002) A1092, https://doi.org/10.1149/1.1491237.
[59] Á. García, M. Retuerto, C. Dominguez, L. Pascual, P. Ferrer, D. Gianolio, A. Serrano, P. Aßmann, D.G. Sanchez, M.A. Peña, S. Rojas, Fe doped porous triazine as efficient electrocatalysts for the oxygen reduction reaction in acid electrolyte, Appl. Catal. B Environ. 264 (2020) 118507, https://doi.org/10.1016/j.apcatb.2019.118507.
[60] M. Retuerto, F. Calle-Vallejo, L. Pascual, G. Lumbeeck, M.T. Fernandez-Diaz, M. Croft, J. Gopalakrishnan, M.A. Peña, J. Hadermann, M. Greenblatt, S. Rojas, La1.5Sr0.5NiMn0.5Ru0.5O6 double perovskite with enhanced ORR/OER bifunctional catalytic activity, ACS Appl. Mater. Interfaces 11 (2019) 21454–21464, https://doi.org/10.1021/acsami.9b02077.
[61] M. Christy, H. Rajan, H. Lee, I. Rabani, S.M. Koo, S.C. Yi, Surface engineering of perovskites for rechargeable zinc-air battery application, ACS Appl. Energy Mater. 4 (2021) 1876–1886, https://doi.org/10.1021/acsaem.0c02983.
[62] J. Il Jung, H.Y. Jeong, J.S. Lee, M.G. Kim, J. Cho, A bifunctional perovskite catalyst for oxygen reduction and evolution, Angew. Chemie - Int. Ed. 53 (2014) 4582–4586, https://doi.org/10.1002/anie.201311223.
[63] Y. Gorlin, T.F. Jaramillo, A bifunctional nonprecious metal catalyst for oxygen reduction and water oxidation, J. Am. Chem. Soc. 132 (2010) 13612–13614, https://doi.org/10.1021/ja104587v.
[64] Y. Zhan, C. Xu, M. Lu, Z. Liu, J.Y. Lee, Mn and Co co-substituted Fe3O4 nanoparticles on nitrogen-doped reduced graphene oxide for oxygen electrocatalysis in alkaline solution, J. Mater. Chem. A. 2 (2014) 16217–16223, https://doi.org/10.1039/C4TA03472D.
[65] J. Yu, Q. He, G. Yang, W. Zhou, Z. Shao, M. Ni, Recent advances and prospective in ruthenium-based materials for electrochemical water splitting, ACS Catal. 9 (2019) 9973–10011, https://doi.org/10.1021/acscatal.9b02457.
[66] K. Wang, Y. Wang, B. Yang, Z. Li, X. Qin, Q. Zhang, L. Lei, M. Qiu, G. Wu, Y. Hou, Highly active ruthenium sites stabilized by modulating electron-feeding for sustainable acidic oxygen-evolution electrocatalysis, Energy Environ. Sci. 15 (2022) 2356–2365, https://doi.org/10.1039/D1EE03610F.
[67] T. Reier, M. Oezaslan, P. Strasser, Electrocatalytic oxygen evolution reaction (OER) on Ru, Ir, and Pt catalysts: a comparative study of nanoparticles and bulk materials, ACS Catal. 2 (2012) 1765–1772, https://doi.org/10.1021/cs3003098.
[68] S. Czioska, A. Boubnov, D. Escalera-López, J. Geppert, A. Zagalskaya, P. Röse, E. Saraçi, V. Alexandrov, U. Krewer, S. Cherevko, J. Grunwaldt, Increased Ir–Ir interaction in iridium oxide during the oxygen evolution reaction at high potentials probed by operando spectroscopy, ACS Catal. 11 (2021) 10043–10057, https://doi.org/10.1021/acscatal.1c02074.
[69] L. Yang, H. Chen, L. Shi, X. Li, X. Chu, W. Chen, N. Li, X. Zou, Enhanced iridium mass activity of 6H-phase, Ir-based perovskite with nonprecious incorporation for acidic oxygen evolution electrocatalysis, ACS Appl. Mater. Interfaces 11 (2019) 42006–42013, https://doi.org/10.1021/acsami.9b11287.
[70] L. Yang, G. Yu, X. Ai, W. Yan, H. Duan, W. Chen, X. Li, T. Wang, C. Zhang, X. Huang, J.-S. Chen, X. Zou, Efficient oxygen evolution electrocatalysis in acid by a perovskite with face-sharing IrO6 octahedral dimers, Nat. Commun. 9 (2018) 5236, https://doi.org/10.1038/s41467-018-07678-w.
[71] M.K. Awasthi, R.K. Rai, S. Behrens, S.K. Singh, Low-temperature hydrogen production from methanol over a ruthenium catalyst in water, Catal. Sci. Technol. 11 (2021) 136–142, https://doi.org/10.1039/d0cy01470b.
[72] D.J. Morgan, Resolving ruthenium: XPS studies of common ruthenium materials, Surf. Interface Anal. 47 (2015) 1072–1079, https://doi.org/10.1002/sia.5852.
[73] H. Wang, X. Li, Q. Ruan, J. Tang, Ru and RuO: X decorated carbon nitride for efficient ammonia photosynthesis, Nanoscale 12 (2020) 12329–12335, https://doi.org/10.1039/d0nr02527e.
[74] M.F. Liu, Z.Z. Du, Y.L. Xie, X. Li, Z.B. Yan, J.M. Liu, Unusual ferromagnetism enhancement in ferromagnetically optimal manganite La0.7-yCa0.3+yMn1-yRuyO3 ($0 \leq y < 0.3$): the role of Mn-Ru t2g super-exchange, Sci. Rep. 5 (2015) 15–16, https://doi.org/10.1038/srep09922.
[75] X. Yu, S. Jin, H. Li, X. Guan, X. Gu, X. Liu, High room-temperature TCR and MR of La1-xSrxMnO3 thin films for advanced uncooled infrared bolometers and magnetic sensors, Appl. Surf. Sci. 570 (2021) 151221, https://doi.org/10.1016/j.apsusc.2021.151221.
[76] A. Machocki, T. Ioannides, B. Stasinska, W. Gac, G. Avgouropoulos, D. Delimaris, W. Grzegorczyk, S. Pasieczna, Manganese-lanthanum oxides modified with silver for the catalytic combustion of methane, J. Catal. 227 (2004) 282–296, https://doi.org/10.1016/j.jcat.2004.07.022.

[77] E. Talik, M. Kruczek, H. Sakowska, Z. Ujma, M. Gała, M. Neumann, XPS characterisation of neodymium gallate wafers, J. Alloys Compd. 377 (2004) 259–267, https://doi.org/10.1016/j.jallcom.2004.01.037.
[78] F. Meng, N. Lin, T. Xia, J. Wang, Z. Shi, J. Lian, Q. Li, H. Zhao, F. Ma, Neodymium-doped ceria nanomaterials: facile low-temperature synthesis and excellent electrical properties for IT-SOFCs, RSC Adv. 3 (2013) 6290–6294, https://doi.org/10.1039/c3ra22833a.
[79] H. Brunckova, H. Kolev, M. Kanuchova, X-ray photoelectron spectroscopy study of neodymium niobate and tantalate precursors and thin films, Surf. Interface Anal. 51 (2019) 326–335, https://doi.org/10.1002/sia.6583.
[80] K. Shigemi, H. Shigenori, A. Hideaki, H. Shin-ichir, S. Kentaro, K. Wasa, Electron spectroscopy of Nd2-xCexCuO4−y (x=0, 0.15, and 0.23) thin films, J. Phys. Soc. Japan. 58 (1989) 4139–4146, https://doi.org/10.1143/JPSJ.58.4139.
[81] S. Song, H. Zhang, X. Ma, Z. Shao, R.T. Baker, B. Yi, Electrochemical investigation of electrocatalysts for the oxygen evolution reaction in PEM water electrolyzers, Int. J. Hydrogen Energy 33 (2008) 4955–4961, https://doi.org/10.1016/j.ijhydene.2008.06.039.
[82] J. Cheng, H. Zhang, G. Chen, Y. Zhang, Study of IrxRu1−xO2 oxides as anodic electrocatalysts for solid polymer electrolyte water electrolysis, Electrochim. Acta 54 (2009) 6250–6256, https://doi.org/10.1016/j.electacta.2009.05.090.
[83] L. Cao, Q. Luo, J. Chen, L. Wang, Y. Lin, H. Wang, X. Liu, X. Shen, W. Zhang, W. Liu, Z. Qi, Z. Jiang, J. Yang, T. Yao, Dynamic oxygen adsorption on single-atomic Ruthenium catalyst with high performance for acidic oxygen evolution reaction, Nat. Commun. 10 (2019) 1–9, https://doi.org/10.1038/s41467-019-12886-z, 2019 101.